Regular Article

Study of Polymer Nanofilms Using for High-Throughput Screening in the Development of Transdermal Therapeutic System

Takahiro Suzuki,* Kanae Sato, Tomohiro Seki, and Toshinobu Seki

Faculty of Pharmaceutical Sciences, Josai University; 1–1 Keyakidai, Sakado, Saitama 350–0295, Japan.
Received June 24, 2022; accepted September 17, 2022

We investigated polymer nanofilm (PNF) for use in high-throughput screening (HTS) to promote the development of transdermal therapeutic systems (TTS). The drug permeability of PNF with a 1 : 1 weight mix ratio of poly(L-lactic acid) (PLLA) and poly(methylhydrosiloxane) (PMHS) (PLLA/PMHS (1/1) PNF) and Strat-M® of the transdermal diffusion test membrane, was evaluated using 12 kinds of drugs with the logarithmic value of *n*-octanol/water partition coefficients of −4.70 to 3.86. The lag time of PLLA/PMHS (1/1) PNF made *via* polymer alloying was significantly shorter than that of Strat-M® for 10 drug types, and the formation of a highly diffusible PMHS-rich phase accompanying the formation of a sea–island structure was suggested as a contributing factor. Additionally, a high correlation was confirmed between the measured value for the logarithm of the apparent permeability coefficient of PLLA/PMHS (1/1) PNF and the literature values for the logarithm of the apparent permeability coefficient of human skin ($r = 0.929$). This study shows that PLLA/PMHS (1/1) PNF can reliably predict drug permeability in human skin and can potentially be used in HTS for developing TTS.

Key words polymer nanofilm; high-throughput screening; artificial membrane; transdermal

Introduction

Since the Food and Drug Administration approved transdermal therapeutic systems (TTS) using scopolamine in 1979, various TTS have been used. For example, clonidine, nitroglycerin, and fentanyl, are used as active ingredients and are used in treating hypertension, angina, or pain.[1] TTS offers the advantage of ease of the administration; unlike injections, it can be administered by application to the skin, which improves patient compliance. In addition, TTS enhances bioavailability compared with oral administration, in addition to decreasing damage to the digestive tract.[2,3] Due to the highlighted benefits of TTS, the market has been on a significant upward trend in recent years, and it is expected that the development of novel TTS will be further promoted in the future.[4,5] However, since the drug permeability of the skin is typically low, it is necessary to select from many candidates by screening for compounds that have potential for development, but the variety of new drug candidate compounds is enormous, so high-throughput testing is desired. To select and optimize for new drug candidate compounds, it is important to select an *in vitro* experimental system considering the cost, time reduction, and controllability of experimental conditions.[6–9] Above all, using an artificial membrane for *in vitro* skin permeation experiment provides good repeatability, material stability, low variability, or high-cost-effectiveness. Moreover, the use of artificial membranes is also effective from the viewpoint of protection of animals. In recent years, the use of Strat-M®, an artificial membrane manufactured by Merck Millipore (Burlington, MA, U.S.A.), has become popular for skin diffusion tests in the early stages of TTS development. Skin permeability is reportedly predictable for hydrophilic and lipophilic drugs. However, there is not much discussion about the time required per penetration assessment test.[10–13] Information about the drug permeation flux of the skin is crucial for predicting efficacy and toxicity, supporting the development of new TTS.[9,14] Predicting the steady-state permeation rate of drugs through the skin in a short time is necessary for high-throughput screening (HTS). Thus, the lag time related to the steady-state arrival time for various drugs of the artificial membranes for which the transdermal absorbability is evaluated is an important parameter in the test method selection in TTS development. Studies related to HTS for the calculation of the permeability profiles of drugs are mainly conducted in the development of oral formulations. For instance, methods using the parallel artificial membrane permeation assay system are well known. In contrast to the development of oral formulations, only a few studies related to the development of TTS have been reported. Therefore, it is necessary to suggest new methods for TTS.[9,15]

Accordingly, we focused on a polymer nanofilm (PNF). PNF is a type of medical material that has been attracting attention recently, and research on wound dressing, tissue engineering, and health-care monitoring is being conducted by taking advantage of its characteristics of being flexible, adhesive, and tailorable. However, the drug permeability of PNF remains unclear. The thickness of PNF is in the nanometer range. Therefore, as predicted from equation (1), the lag time is expected to be short.[16–18]

$$T_{\mathrm{lag}} = \frac{L^2}{6D_{\mathrm{app}}} \tag{1}$$

T_{lag} represents the lag time, L represents the film thickness of the evaluated membrane, and D_{app} represents the apparent diffusion coefficient.[12,19] Moreover, it is expected that the drug permeability of PNF will change significantly due to the mixing of multiple component polymers, that is, the use of polymer alloy. If phase separation occurs because of the mixing of multiple types of polymers within a polymer alloy, the permeation pathways for a specific phase may be separated or mul-

* To whom correspondence should be addressed. e-mail: gyd1902@josai.ac.jp

tiple permeation pathways may be formed. Therefore, polymer alloys have potential for controlling the drug permeation of PNF, leading to short lag times and high functionality.

In this study, we investigated the PNFs that can be used for HTS in the development of TTS. Various PNFs were created using poly(L-lactic acid) (PLLA) and poly(methylhydrosiloxane) (PMHS) as the component polymers. Thereafter, the drug permeability was evaluated using various drugs with the logarithmic value of *n*-octanol/water partition coefficients ($\log K_{ow}$) of −4.70 to 3.86. We compared the lag times with that for Strat-M®, and correlated it with published data on the logarithm of the apparent permeability coefficient of the human skin ($\log P_{hum}$).[20] This allowed the selection of a PNF that can be used reliably for predicting drug permeability across human skin, which can be subsequently used for HTS.

Experimental

Materials Poly(L-lactic acid) (PLLA) (Mw approx., 90000) was purchased from Polymer Science Inc. (Monticello, IN, U.S.A.). Poly(methylhydrosiloxane) (Mn 1700–3200) (PMHS), poly(diallyldimethylammonium chloride) (PDAC) were purchased from Sigma-Aldrich (St. Louis, MO, U.S.A.). Polyethylene glycol 400, poly(vinyl alcohol) (PVA), ketoprofen (KP), acetonitrile, 1-octanesulfonic acid sodium salt, sodium dodecyl sulfate, phosphoric acid were obtained from FUJIFILM Wako Pure Chemical Corporation (Osaka, Japan). Flurbiprofen (FP), indomethacin (IDM), lidocaine (LC), cyclobarbital (CB), aminopyrine (AMP), 5-fluorouracil (5-FU), diclofenac sodium (DC-Na), antipyrine (ANP), isoproterenol hydrochloride (IPH), dopamine hydrochloride (DPH), levodopa (L-DP), tetra-*n*-butylammonium hydrogensulfate, methyl paraben, ethyl paraben, *n*-propylparaben, *n*-butylparaben were purchased from Tokyo Chemical Industry Co., Ltd. (Tokyo, Japan). Filtration filter (pore size 0.45 μm, olefin series polymer) was obtained from TOSC Japan Ltd. (Tokyo, Japan). Strat-M® was purchased from Merck Millipore (Burlington, MA, U.S.A.). Silicon wafer was obtained from Takeda Rika Kogyo Co., Ltd. (Tokyo, Japan).

Preparation of Polymer Nanofilm Using the Spin-Coating Method PNF was prepared using the spin coating method.[21–23] PNF of pure PLLA (PLLA PNF), PNF with a 3 : 1 mass mixture ratio of PLLA and PMHS (PLLA/PMHS (3/1) PNF), and PNF with a 1 : 1 mass mixture ratio of PLLA and PMHS (PLLA/PMHS (1/1) PNF) were prepared. Figure 1 shows a schematic diagram of how to create PNFs. The spin coater used Opticoat (MS-B100, Mikasa Co., Ltd., Tokyo, Japan). The hot plate (HSH-1D, AS ONE Co., Osaka, Japan) was used to dry the PNF at 70 °C. The silicon substrate (Si substrate) was used by cutting out a piece 3.5 cm from one side of the silicon wafer. The composition of the pre-sacrificial layer solution was 5 mg/mL PVA/10 mg/mL PDAC, with water as the solvent. The pre-PNF solution contained 40 mg/mL PLLA, 30 mg/mL PLLA/10 mg/mL PMHS, or 20 mg/mL PLLA/20 mg/mL PMHS. Dichloromethane was used as the solvent. One milliliter of 5 mg/mL PVA/10 mg/mL PDAC solution was dropped onto the silicon substrate, spin-coated under the conditions of 4000 rpm and 20 s by Opticoat (MS-B100, Mikasa Co.), and dried under the conditions of 70 °C and 90 s. Then, 1 mL of 40 mg/mL PLLA, 30 mg/mL PLLA/10 mg/mL PMHS, or 20 mg/mL PLLA/20 mg/mL PMHS solution was dropped onto the substrate, spin coated at 4000 rpm for 20 s, and dried at 70 °C for 90 s. After drying, PNF was peeled off in water to prepare PNFs for membrane permeation test. The prepared PNFs were attached to a silicone ring (Fuso Rubber Co., Ltd., Hiroshima, Japan, inner diameter; 20 mm, outer diameter; 30 mm) and dried in an incubator (LWO-600, TOKYO RIKAKIKAI Co., Ltd., Tokyo, Japan) at 30 °C for 12 h. The prepared PNF was stored in a desiccator (AS ONE Co.) and used within 2 weeks of preparation. Care was taken not to affect the PNF state (pore state, membrane morphology, *etc.*) by handling the site of the silicone ring.

Measurement of Non-contact Film Thickness The PNF thickness was measured by coating the silicon substrate directly and using the film thickness monitor (FE-300, Otsuka Electronics Co. Ltd., Osaka, Japan). Aluminum was used as the reference, the wavelength ranged from 450 to 800 nm, and the film thickness was measured in the absolute reflectance mode.

Measurement Using HPLC The drugs were analyzed using HPLC with the Shimadzu HPLC Class 10A series. The conditions corresponding to various drugs are listed in Supplementary Table S1. The LC-10AT pump was set to a flow rate of 0.25 mL/min. The reverse-phase HPLC columns Mightysil RP-18 GP (150 × 2.0 mm i.d., particle size 3 μm, Kanto Chemical Co., Inc., Tokyo, Japan) and guard column Mightysil RP-18 GP (5 × 2.0 mm i.d., particle size 3 μm, Kanto Chemical Co., Inc.) were used. The column temperature was set at 45 °C using HIC-6A column oven (Shimadzu, Kyoto, Japan). The prepared samples were injected into the flow channel using SCL-6B system controller and auto-injector (Shimadzu). The concentration of the drug was determined using the internal standard method in HPLC.

***In Vitro* Permeation Test** *In vitro* permeability experiment was performed using the Franz-type diffusion cells. Evaluation

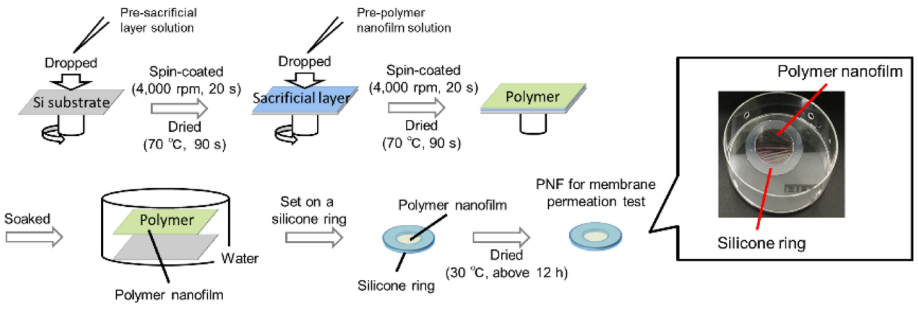

Fig. 1. Schematic Showing Polymer Nanofilm Preparation Using the Spin-Coating Method

system configuration was described to Supplementary Fig. S1. The drug solution or suspension were added to the donor site, and distilled water, or 40% polyethylene glycol solution was added to the receiver site. The calculation of the drug permeation flux requires the maintenance of sink conditions at the receiver site for the duration of the test. The solubilities of FP, IDM, and KP in water are poor, which renders the maintenance of sink conditions challenging. Therefore, per previous reports, 40% polyethylene glycol solution was used for evaluating these drugs.[15,20] A glass filter (pore size: approximately 1 μm, GS-25, Advantec Toyo Kaisha, Ltd., Tokyo, Japan) was used as a support when PNF was used for evaluation. The effective surface area was 3.14 cm^2, and the holding temperature was 32 °C. Twelve kinds of drugs ($\log K_{ow}$ −4.70 to 3.86, M.W. 130 to 318) were used to assess the permeability.[24] PLLA PNF, PLLA/PMHS (3/1) PNF, PLLA/PMHS (1/1) PNF, and Strat-M® (film thickness; 300 μm) were the evaluated membranes. The PNF with 3 : 5 mass mixture ratio of PLLA and PMHS [PLLA/PMHS (3/5)] was 521 ± 13 nm thick (mean ± standard deviation (S.D.), $n = 3$). However, many pores formed with diameters of several micrometers or more (Supplementary Fig. S5). This largely reflects the characteristics of a porous membrane. Unlike that observed for the skin, the difference in the *n*-octanol/water partition coefficient of drugs is difficult to discern when using porous membranes.[24] Therefore, PLLA/PMHS (3/5) PNF was not suitable as a skin model membrane. The drug concentration was quantified by HPLC method. The concentration of the applied suspension was filtered through the membrane filter (pore size 0.45 μm, olefin series polymer) to quantify the drug concentration in the filtrate. The types of drugs, abbreviations, molecular weights, and $\log K_{ow}$, concentrations of applied drugs are described in Table 1. In this experiment, for convenience, drugs with $\log K_{ow} \geq 0$ was defined as lipophilic drugs, and drugs with $\log K_{ow} < 0$ was defined as hydrophilic drugs. The drug permeation flux was calculated from the steady-state portion of the permeation profile, and the apparent permeability coefficient was calculated by dividing the drug permeation flux by the initial concentration of the applied drug. The lag time was calculated from the intersection of the steady-state slope and the time axis (*X*-axis) in the permeation profile.[12,19] Moreover, the following formula (2) was used to calculate the *DK* parameter (*DK*), which is the value obtained by correcting the apparent permeability coefficient of the artificial film by the film thickness.

$$DK = P_{app}L \quad (2)$$

P_{app} represents the apparent permeability coefficient, and L represents the film thickness.[12,19]

Observation of Polymer Distribution in Polymer Nanofilm Using Raman Microscopy One milliliter of the pre-PNF solution (20 mg/mL PLLA/20 mg/mL PMHS; solvent, dichloromethane) was added dropwise to an aluminum flat mirror (Sigmakoki Co., Ltd., Tokyo, Japan), spin-coated (4000 rpm, 20 s) using Opticoat, and dried at 70 °C for 90 s on the hot plate (HSH-1D). Subsequently, polymer distribution was observed using a Raman microscope (XploRA PLUS, Horiba, Ltd., Kyoto, Japan). The wavelength of the laser was 532 nm, the acquisition time was 3 s, the measurement step was 0.2×0.2 μm, and the total measurement time was 2 h. Mapping images were obtained using the classical least squares method utilizing a reference spectrum for each component.

Measurement with Field Emission Scanning Microscope and Energy Dispersive X-Ray Spectroscopy The membrane morphology and polymer distribution were observed using the field emission scanning microscope (FE-SEM) and energy dispersive X-ray analysis (EDS). The equipment was used JSM-IT800(SHL) (JEOL Ltd., Tokyo, Japan). The evaluated samples are the prepared PNFs for membrane permeation testing. The sample was platinum coated by the vapor deposition method. The acceleration voltage at the time of observation was 15 kV.

Statistical Processing The regression line and the coefficient of determination (R^2) were determined using the analysis tools of Excel office 2019 (version 2203, Microsoft Co., Ltd., MS, U.S.A.). Statistical significance between two groups was evaluated using Dunnett's test, Tukey–Kramer test, and correlation was evaluated using Pearson's correlation coefficient (r). BellCurve® for Excel (version 3.21, Social Information Service, Tokyo, Japan) was used for calculation.

Results and Discussion

Comparison of Permeability to Indomethacin Figure 2a

Table 1. Drug Species Used for *in Vitro* Permeation Test and, Abbreviation, Molecular Weight (M.W), Logarithmic Values of *n*-Octanol/Water Partition Coefficient (Log K_{ow}), and Concentration of Applied Drug Solution

Chemical	Abbreviation	M.W.[a]	$\log K_{ow}$[a]	Applied drug concentration (mg/mL)[b]
Flurbiprofen	FP	244	3.86	0.0282 ± 0.0005
Indomethacin	IDM	358	3.19	0.00199 ± 0.00017
Ketoprofen	KP	254	3.11	0.166 ± 0.003
Lidocaine	LC	234	2.37	3.68 ± 0.14
Cyclobarbital	CB	236	0.873	1.91 ± 0.07
Aminopyrine	AMP	231	0.497	56.5 ± 3.3
5-Fluorouracil	5-FU	130	−0.860	14.3 ± 0.3
Diclofenac sodium	DC-Na	318	−0.962	22.0 ± 0.6
Antipyrine	ANP	188	−1.55	101 ± 2
Isoproterenol hydrochloride	IPH	248	−2.69	100 ± 1
Dopamine hydrochloride	DPH	190	−3.40	101 ± 2
Levodopa	L-DP	197	−4.70	4.80 ± 0.07

a) Hatanaka T., Inuma M., Sugibayashi K., Morimoto Y., *Chem. Pharm. Bull.*, **38**, 3452–3459 (1990) (the logarithmic value of *n*-octanol/water partition coefficient at 37 °C). *b*) Solubility in water at 32 °C (mean ± S.D., $n = 3$–4).

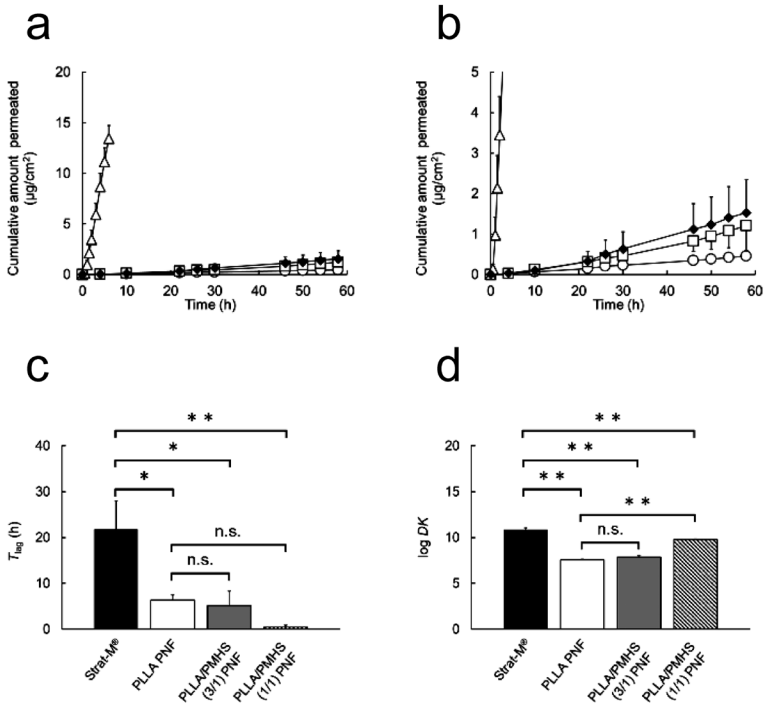

Fig. 2. Drug Permeation Profiles ((a), (b); (b) Is Enlarged View of (a)) and Calculated Lag Times (T_{lag}) (c) of Strat-M® (◆), PLLA PNF (○), PLLA/PMHS (3/1) PNF (□), and PLLA/PMHS (1/1) PNF (△) for Indomethacin; (d) Comparison of Logarithmic Values of *DK* Parameters (Log*DK*)

Error bars indicate standard deviation ($n = 3$, significant difference, $*p < 0.05$, $**p < 0.01$).

show the drug permeability profile of IDM across Strat-M® and the prepared PNFs. Figure 2b shows an enlarged view of Fig. 2a. The cumulative amount of IDM increased in a time-dependent manner, eventually achieving a steady state. The calculated lag time is shown in Fig. 2c. PLLA PNF (mean thickness ± S.D., 801 ± 55 nm; $n = 3$), PLLA/PMHS (3/1) PNF (mean thickness ± S.D., 609 ± 3 nm; $n = 3$), and PLLA/PMHS (1/1) PNF (mean thickness ± S.D., 527 ± 2 nm; $n = 3$) showed significantly shorter lag time than Strat-M®. On this basis, we expected that the lag time could be shortened by converting an artificial membrane to PNF. Indeed, the use of polymer alloying further shortened the lag time. Interestingly, the difference in the ratio of PLLA and PMHS during preparation affected the lag time, and PLLA/PMHS (1/1) PNF showed the shortest lag time. In addition, the calculated drug permeation flux (mean ± S.D., $n = 3-4$) was $4.04 \times 10^{-2} \pm 1.67 \times 10^{-2}$ μg/cm²/h for Strat-M®, $8.70 \times 10^{-3} \pm 9.42 \times 10^{-4}$ μg/cm²/h for PLLA PNF, $2.14 \times 10^{-2} \pm 8.76 \times 10^{-3}$ μg/cm²/h for PLLA/PMHS (3/1) PNF, and $2.53 \pm 4.03 \times 10^{-1}$ μg/cm²/h for PLLA/PMHS (1/1) PNF. These results showed that differences in the PLLA and PMHS ratios affected the drug permeation flux, and that PLLA/PMHS (1/1) PNF showed significantly higher drug permeation flux than Strat-M®. Therefore, we suggest that PLLA/PMHS (1/1) PNF, generated using polymer alloying, will be effective for HTS during TTS development.

Figure 2d shows the logarithmic value of *DK* (log*DK*), a value obtained by correcting the apparent permeability coefficient of the artificial membrane by the film thickness. Log *DK* did not differ significantly between PLLA PNF and PLLA/PMHS (3/1) PNF. In contrast, significant differences in log*DK* were observed between PLLA PNF and PLLA/PMHS (1/1) PNF. Therefore, we concluded that the change in drug permeability of PLLA/PMHS (1/1) PNF occurred because of factors other than the change in film thickness. PLLA/PMHS (1/1) PNF generated using polymer alloying may have significantly changed membrane properties compared with those of PLLA PNF. Therefore, in subsequent analyses, we focused on the drug permeability of PLLA/PMHS (1/1) PNF, which showed the best performance.

Permeability of PNF to Drugs of Different Polarities Table 2 shows the statistical significance difference of lag time to various drugs of PLLA and PLLA/PMHS (1/1) PNF, comparison to Strat-M®. Strat-M® could not be evaluated for IPH, DPH, and L-DP of $\log K_{ow} < -2.0$, because those were below the detection limit in the 48-h permeation experiment. Compared to Strat-M®, PLLA PNF provided the significantly shorter lag time for nine drugs. In contrast, PLLA/PMHS (1/1) PNF provided the significantly shorter lag time for the 10 drug types. Supplementary Figure S2 shows the relationship graph between the lag times and the $\log K_{ow}$ of applied drugs. Looking at the relationship graph between lag time and $\log K_{ow}$ of the applicable drug, PLLA PNF and PLLA/PMHS (1/1) PNF have miniscule lag times for KP, IDM, and FP with $\log K_{ow} > 3.0$, compared to Strat-M®. Moreover, the DPH, IPH, L-DP of $\log K_{ow} < -2.0$ were evaluable by PNFs. Therefore, compared with Strat-M®, the permeabilities of highly lipophilic or hydrophilic drugs, such as those with $\log K_{ow} > 3.0$ or $\log K_{ow} < -2.0$, could be assessed in a high throughput manner using various PNFs.

The short lag times of these PNFs than that of Strat-M® may be because of the nanometer-range thickness of these films. Equation (1) shows that the lag time decreased with a reduction in film thickness. The film thicknesses of PLLA PNF and PLLA/PMHS (1/1) PNF (mean ± S.D., $n = 3$) were 801 ± 55 nm and 527 ± 2 nm, the Strat-M® film thickness was 300 μm.

Table 2. List of Lag Times (T_{lag}) for Strat-M®, PLLA PNF, and PLLA/PMHS (1/1) PNF for 9 or 12 Kinds of Drugs with Different Polarities[a)]

Membrane	Strat-M®		PLLA PNF		PLLA/PMHS (1/1) PNF	
Drug	T_{lag} (h)		T_{lag} (h)		T_{lag} (h)	
FP ($\log K_{ow}$ 3.86,M.W. 244)	33.2 ± 7.0	—	13.2 ± 0.1	**	0.813 ± 0.288	**
IDM ($\log K_{ow}$ 3.19,M.W. 358)	21.7 ± 6.3	—	6.37 ± 1.11	**	0.645 ± 0.162	**
KP ($\log K_{ow}$ 3.11,M.W. 254)	17.4 ± 5.0	—	8.78 ± 3.10	*	1.34 ± 0.04	**
LC ($\log K_{ow}$ 2.37,M.W. 234)	0.686 ± 0.229	—	2.07 ± 0.95	*	0.151 ± 0.067	n.s.
CB ($\log K_{ow}$ 0.873, M.W. 236)	0.835 ± 0.124	—	2.10 ± 1.23	n.s.	0.214 ± 0.114	n.s.
AMP ($\log K_{ow}$ 0.497, M.W. 231)	1.01 ± 0.11	—	0.767 ± 0.016	**	0.0455 ± 0.0281	**
5-FU ($\log K_{ow}$ −0.860, M.W. 130)	3.69 ± 1.14	—	1.63 ± 0.64	**	0.108 ± 0.045	**
DC-Na ($\log K_{ow}$ −0.962, M.W. 318)	0.628 ± 0.036	—	0.837 ± 0.184	n.s.	0.107 ± 0.070	**
ANP ($\log K_{ow}$ −1.55, M.W. 188)	1.04 ± 0.08	—	0.302 ± 0.182	**	0.0450 ± 0.0281	**
IPH ($\log K_{ow}$ −2.69, M.W. 248)	—[b)]	—	0.121 ± 0.061	—	0.126 ± 0.072	—
DPH ($\log K_{ow}$ −3.40, M.W. 190)	—[b)]	—	0.245 ± 0.055	—	0.0712 ± 0.0261	—
L-DP ($\log K_{ow}$ −4.70, M.W. 197)	—[b)]	—	1.31 ± 0.32	—	0.237 ± 0.071	—

a) Errors indicate standard deviation ($n = 3$–4, significant differences compared with Strat-M®, $*p < 0.05$, $**p < 0.01$). *b*) No permeability of the drugs through the membranes was detected until 48 h (Strat-M®; IDP, DPH, L-DP).

Therefore, we concluded that the nanometer-range thickness of these films enabled the short lag times. In contrast, the drug permeation flux or the apparent permeability coefficients of Strat-M®, PLLA PNF, and PLLA/PMHS (1/1) PNF for the 12 drug types (Supplementary Table S2 and Table S3), and the $\log DK$ values of PLLA PNF and PLLA/PMHS (1/1) PNF for the 12 drugs (Supplementary Table S4), indicated that polymer alloying affected the drug permeability of PNF, resulted in miniscule lag times, owing to the high permeability for the 12 drug types with different polarities. The drug permeabilities of PLLA PNF and PLLA/PMHS (1/1) PNF may differ because of differences in film thicknesses. However, a comparison of *DK* parameters confirmed the significant differences among the 12 drug types. Therefore, changes in drug permeability may be due to factors other than film thickness, that is, changes in drug diffusivity and partition of the membrane in PNF due to polymer alloying. This may involve the formation of a phase-separated structure within the PNF.

Therefore, the PLLA and PMHS structures were evaluated using Raman microscopy. Figure 3 shows a mapping image of PLLA/PMHS (1/1) PNF observed using Raman microscopy. PLLA is denoted by the red area and PMHS is denoted by the blue area. The results confirmed that both PLLA and PMHS formed a rich phase, suggesting that PLLA/PMHS (1/1) PNF may form sea–island structures. Furthermore, the presence of the miscible region, represented as mixed red and blue areas, confirmed that the PLLA/PMHS (1/1) PNF formed a partially compatible state. Supplementary Figure S3 shows the differential scanning calorimetry (DSC) curves of PLLA powder, PLLA PNF, and PLLA/PMHS (1/1) PNF. The PLLA-derived glass-transition temperature (T_g) of PLLA/PMHS (1/1) PNF was observed as 58 °C, which was slightly lower than the T_g of PLLA PNF (60 °C). The DSC results indicated that PLLA/PMHS (1/1) PNF formed a partially compatible state, corroborating the results of Raman microscopy.[25)] Therefore, the formation of a partially compatible state *via* polymer alloying resulted in the formation of sea–island structures within the PNF, which may affect the partitioning of the membrane and drug diffusivity across the membrane. In particular, we believe that the formation of the PMHS-rich phase induced by polymer alloying was important for the changes in drug permeability.

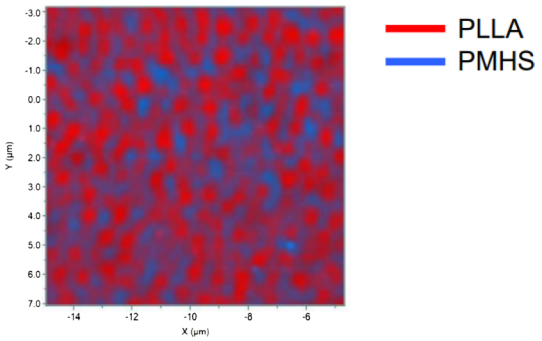

Fig. 3. Mapping Image of PLLA/PMHS (1/1) PNF Obtained Using the Raman Microscope (PLLA: Red Area; PMHS: Blue Area)

Material diffusion through the component polymer of the artificial membrane is affected by the free volume change of the polymer. Temperatures above T_g of the constituent polymers, it is expected that the segmental motion of the constituent polymers will become very active, the free volume will increase in a temperature-dependent manner, and the material diffusivity in the membrane will become very high.[26,27)] PMHS is a liquid silicone oil that is transparent at 20 °C and is a highly lipophilic polymer. Additionally, T_g of PMHS is very low at −135 °C, with very high segment motion occurring at the experimental temperature of 32 °C, hence, the free volume is considered large for PMHS in PLLA/PMHS (1/1) PNF.[28)] Therefore, the mixing of PMHS may have resulted in the formation of the PMHS-rich phase, with large free volume in PLLA/PMHS (1/1) PNF, which affected the drug diffusivity in PNF, thereby resulting in short lag times. In contrast, the formation of PMHS-rich phase comprising PMHS for the lipophilic polymer may also have altered the partition of the membrane of the drug.

Figure 4 shows the film morphology image of FE-SEM and the mapping images of the elements observed by EDS. Changes in film morphology were observed because of polymer alloying. In addition, non-uniformity was confirmed in the distribution of Si, which is a constituent element of PMHS, confirming that PLLA/PMHS (1/1) PNF forms a PMHS-rich phase in the film. We believe that this further supports the formation of a PMHS-rich phase in the PLLA/PMHS (1/1) PNF.

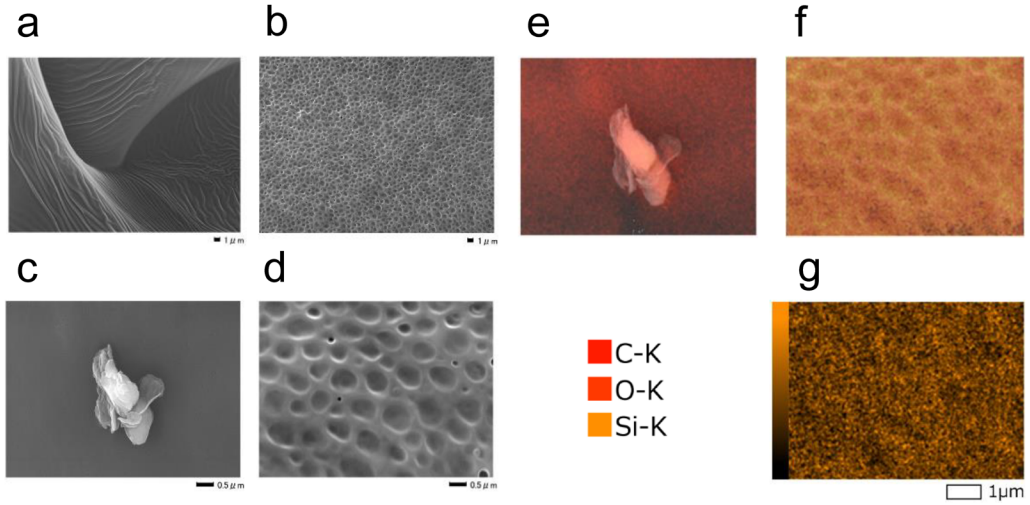

Fig. 4. Morphologies of PLLA PNF and PLLA/PMHS (1/1) PNF Observed Using a Field Emission Scanning Microscope (PLLA PNF, (a), (c); PLLA/PMHS (1/1) PNF, (b), (d)); Elemental Mapping Images of PLLA PNF and PLLA/PMHS (1/1) PNF Observed Using Energy Dispersive X-Ray Analysis (PLLA PNF, (e); PLLA/PMHS (1/1) PNF, (f), (g))

Samples were platinum-coated. (g) Only shows the distribution of Si. The acceleration voltage at the time of observation was 15 kV. The scale bar is 0.5 or 1.0 μm.

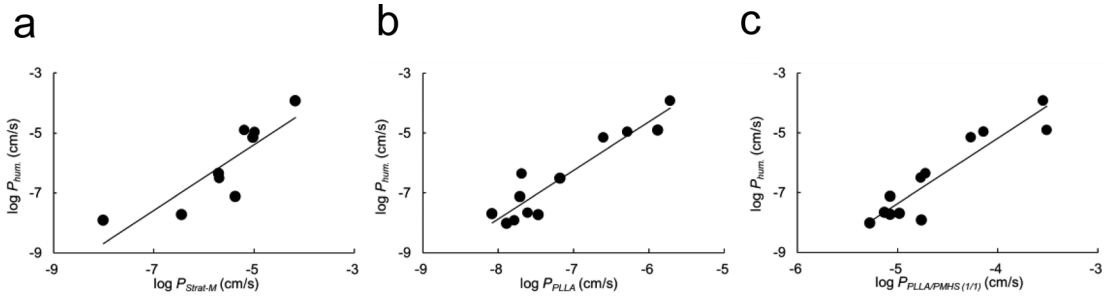

Fig. 5. Relationship between the Logarithmic Value of the Apparent Permeability Coefficient of Human Skin for 9 or 12 Types of Drugs ($\mathrm{Log}P_{hum.}$, Literature Value) and the Logarithmic Value of the Apparent Permeability Coefficient of Strat-M® ($\mathrm{Log}P_{Strat\text{-}M}$), PLLA PNF ($\mathrm{Log}P_{PLLA}$), and PLLA/PMHS (1/1) PNF ($\log P_{PLLA/PMHS\ (1/1)}$) (Strat-M®, (a); PLLA PNF, (b); PLLA/PMHS (1/1) PNF, (c))

The straight line represents the regression line (Strat-M®, $n=9$; PLLA PNF, $n=12$; PLLA/PMHS (1/1) PNF, $n=12$). $\mathrm{Log}P_{hum.}$ was obtained from a previous study (Morimoto Y., Hatanaka T., Sugibayashi K., Omiya H., *J. Pharm. Pharmacol.*, **44**, 634–639 (1992).).

Drug Permeation Similarity with Human Skin Next, we evaluated the drug permeation similarity with the human skin. Supplementary Table S3 shows the measured values of the apparent permeability coefficients of various artificial membranes, and Fig. 5 shows the correlation between $\log P_{hum.}$ and the measured values of the logarithm of apparent permeability coefficients of various artificial membranes ($\log P_{Strat\text{-}M}$, $\log P_{PLLA}$, $\log P_{PLLA/PMHS\ (1/1)}$).[20] Strat-M® was found highly correlated with nine kinds of drugs ($r=0.856$). In contrast, PLLA PNF and PLLA/PMHS (1/1) PNF were found to have very high correlation with the 12 drug types including drugs of $\log K_{ow}<-2.0$ ($r=0.939$, 0.929). Moreover, since PLLA/PMHS (1/1) PNF has the higher drug permeability, it can be evaluated in drugs whose limit of determination is usually a problem, it was considered useful for HTS in the development of TTS.

The formula of the regression line calculated from each result of Fig. 5 is shown below;

$$\log P_{hum.}=1.10\log P_{Strat-M}+0.10\ (R^2=0.743)$$
$$\log P_{hum.}=1.63\log P_{PLLA}+5.14\ (R^2=0.881)$$
$$\log P_{hum.}=2.18\log P_{PLLA/PMHS(1/1)}+3.56\ (R^2=0.860)$$

The slope of Strat-M® was relatively close to 1.0, while the slope of PLLA PNF and PLLA/PMHS (1/1) PNF is approximately 2.0. When artificial membranes were used as the human skin permeability prediction membrane, the larger the slope, the greater is the influence on the results due to changes in the data, however, PLLA/PMHS (1/1) PNF showed the highest correlation coefficient (Fig. 5). Therefore, we believe that predictions can be made with sufficient reliability.

Evaluation of Imitation of Lipid Pathway and Pore Pathway Figure 6 shows the relationship between the $\log K_{ow}$ of various drugs and the logarithm of the apparent permeability coefficient ($\log P_{Strat\text{-}M}$, $\log P_{PLLA}$, $\log P_{PLLA/PMHS\ (1/1)}$). The regression line in the Fig. 6 is represented by the lipophilic drugs ($\log K_{ow}\geq 0$). The results suggest that Strat-M® has the highly correlation coefficient ($r=0.887$) and is suitable for predicting the permeability of lipophilic drugs, in contrast, the prediction accuracy of hydrophilic drugs is low. However, PLLA PNF and PLLA/PMHS (1/1) PNF were found to have high correlation coefficients between $\log K_{ow}$ and the measure value for the logarithm of the apparent permeability coefficient of lipophilic drugs ($r=0.943$, 0.933). Moreover, the measured value for the logarithmic of the apparent permeability coefficients for PLLA PNF and PLLA/PMHS (1/1) PNF for hydro-

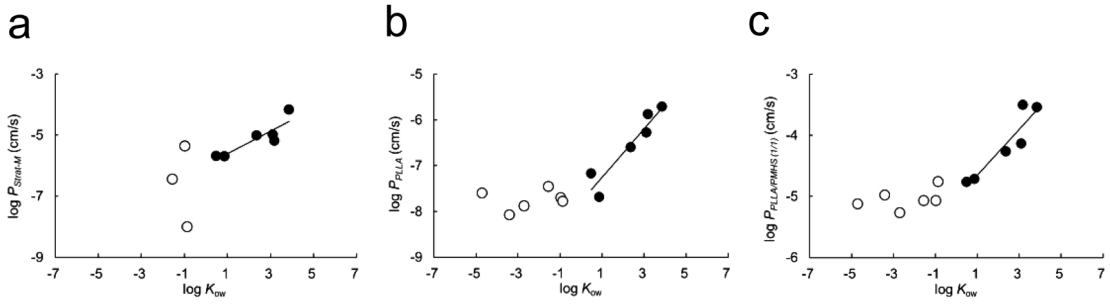

Fig. 6. Relationship between the Logarithmic Value of the Apparent Permeability Coefficient of Strat-M® (Log $P_{Strat\text{-}M}$), PLLA PNF (Log P_{PLLA}), and PLLA/PMHS (1/1) PNF (Log $P_{PLLA/PMHS\ (1/1)}$) to the Logarithmic Value of the *n*-Octanol/Water Partition Coefficient (Log K_{ow}) of 9 or 12 Kinds of Drugs (Strat-M®, (a); PLLA PNF, (b); PLLA/PMHS (1/1) PNF, (c))

The regression line is represented by the lipophilic drug ($\log K_{ow} \geq 0$) site (lipophilic drugs, (●); hydrophilic drugs, (○)).

philic drugs showed constant values. This difference is considered to be due to the difference in the imitation of the lipid pathway and the pore pathway in the membrane. Morimoto *et al.* simplified the drug permeation pathway in the skin with the parallel permeation pathway model that combines the lipid pathway and the pore pathway.[20,24] The model shows that the logarithmic of the apparent permeability coefficients of the lipophilic drug that permeate the lipid pathway correlates with the value of $\log K_{ow}$. In contrast, the logarithmic of apparent permeability coefficients of the hydrophilic drug that permeates the pore pathway does not involve the process of distribution to the membrane components and shows a constant value unless the molecular weights differ significantly. Previous studies have not discussed the existence of drug permeability and the pore pathway for $\log K_{ow} < -2.0$ for Strat-M®.[11–13] The results of this study suggest that Strat-M® is not intended to mimic the pore pathway. However, the logarithmic of the apparent permeability coefficients of PLLA PNF and PLLA/PMHS (1/1) PNF for the hydrophilic drugs showed constant values. Therefore, the pore pathway was mimicked in these membranes, and PNF was considered to be capable of assessing the permeability of IPH, DPH, and L-DP that are categorized as highly hydrophilic drugs.

Figure 4 shows the membrane morphology of PLLA/PMHS (1/1) PNF observed using FE-SEM, which confirmed the formation of small pores several nanometers in diameter. Therefore, we concluded that PLLA/PMHS (1/1) PNF can be used to assess the osmosis of IPH, DPH, and L-DP by allowing the observed pores to function *via* the pore pathway.

The equivalent radius of the membrane pore (R) and the pore occupancy/length ratio (ε/L) of PLLA PNF and PLLA/PMHS (1/1) PNF were determined using the Renkin function.[29–31] A list of parameters used for this calculation is presented in Supplementary Table S5, and the results are listed in Supplementary Table S6. Previous studies have reported that the R associated with the follicular appendageal pathway in the skin is approximately 50–700 μm, while that associated with the transcellular component of the skin's porous pathway during normal and widened states is approximately 0.5–40 nm.[32–34] Therefore, the R of PLLA PNF and PLLA/PMHS (1/1) PNF may be similar to the transcellular component of the skin's porous pathway. In contrast, the reported ε/L is $1.8 \times 10^{-2}\,\mathrm{cm}^{-1}$ for the follicular appendageal pathway in skin and $3.3 \times 10^{-2}\,\mathrm{cm}^{-1}$ for the transcellular component of the skin's porous pathway.[34] Therefore, PLLA/PMHS (1/1) PNF may have a higher pore density than skin; thus, when PLLA/PMHS (1/1) PNF is used as a skin model membrane, attention should be paid to the differences in pore density.

Many drugs used in TTS are lipophilic, and it may appear unnecessary to set the permeation pathway for hydrophilic drugs or predict their permeability. However, the fact that PNF conversion of artificial membrane, and polymer alloying have shown the possibility of imparting various functions and properties to membrane permeability is significant. In certain cases, for example, when the skin is treated with absorption enhancers or when iontophoresis is applied, the hydrophilic permeation pathway is important. In such conditions, the combination of nanofilms and polymer alloying may be useful. In future studies, we plan to assess the adaptability to predicting permeability under conditions of change in drug permeability. When PNF is used to predict the permeation of highly lipophilic drugs, the permeation resistance of the dermal layer should be mimicked. In other words, the formation of a hydrophilic layer is important. We believe that this problem can be solved by lamination formation. For example, we believe that lamina can be formed by coating reported hydrophilic PNFs (such as PNFs formed from chitosan and alginic acid) on PLLA/PMHS (1/1) PNF.[35] We also believe that the permeation resistance of the hydrophilic layer to highly lipophilic drugs is reproducible.

Conclusion

From the results of this study, PLLA/PMHS (1/1) PNF provided significantly shorter lag times compared to Strat-M®, and the polymer alloying PLLA/PMHS (1/1) PNF provided the significantly shorter lag times of 0.045 to 1.3 h for the drugs with different polarities from −4.70 to 3.86 for $\log K_{ow}$. Moreover, the high similarity of the drug permeability to that of the human skin was confirmed, suggesting its usability in HTS for the development of TTS. In contrast, polymer alloying with PLLA and PMHS changes the drug permeability by forming the PMHS-rich phase in PNF and also changing the membrane morphology. Thus, it may be possible to control the phase separation state and membrane morphology in PNF by changing the mixing ratio of PLLA and PMHS, it is considered that PNF with high functionality can be proposed in future additional research. Furthermore, we believe that drugs can be retained in PNF if they are dissolved in the polymer solution during preparation and if the PNF is prepared using spin coating.[18] Therefore, the results of this research will bring about further development not only in the development of HTS using PNFs but also in the creation of new artificial

skin and research on medical materials such as nano-adhesive plasters.

Acknowledgments This research was partly supported by JSPS KAKENHI (Grant No.; 18K06794). Raman microscope imaging of PNF was performed by Horiba, Ltd.

Conflict of Interest The authors declare no conflict of interest.

Supplementary Materials This article contains supplementary materials.

References

1) Prausnitz M. R., Langer R., *Nature Biotechnology*, **26**, 1261–1268 (2008).
2) Bhowmik D., Pusupoleti K. R., Duraivel S., Sampath K. K., *The Pharma Innovation*, **2**, 99–108 (2013).
3) Romita P., Foti C., Calogiuri G., Cantore S., Ballini A., Dipalma G., Inchingolo F., *Acta. Biomed.*, **90**, 5–10 (2019).
4) Pyo S. M., Maibach H. I., *Skin Pharmacol. Physiol.*, **32**, 283–294 (2019).
5) Priyanka M. P., Kinjal P. S., Vipul A. M., *Int. J. Pharm. Clin. Res.*, **10**, 65–73 (2018).
6) Lipinski C. A., *J. Pharmacol. Toxicol. Methods*, **44**, 235–249 (2000).
7) Karande P., Mitragotri S., *Pharm. Res.*, **19**, 655–660 (2002).
8) Ayalasomayajula L. U., Kumari M. K., Earle R. R., *RJTC*, **12**, 4–12 (2021).
9) Sinkó B., Garrigues T. M., Balogh G. T., Nagy Z. K., Tsinman O., Avdeef A., Takács-Novák K., *Eur. J. Pharm. Sci.*, **45**, 698–707 (2012).
10) Ponmozhi J., Dhinakaran S., Varga-medveczky Z., Fónagy K., Bors L. A., Iván K., Erdő F., *Micromachines*, **12**, 1–25 (2021).
11) Haq A., Goodyear B., Ameen D., Joshi V., Michniak-Kohn B., *Int. J. Pharm.*, **547**, 432–437 (2018).
12) Uchida T., Kadhum W. R., Kanai S., Todo H., Oshizaka T., Sugibayashi K., *Eur. J. Pharm. Sci.*, **67**, 113–118 (2015).
13) Uchida T., Nishioka K., Motoki A., Yakumaru M., Sano T., Todo H., Sugibayashi K., *Chem. Pharm. Bull.*, **64**, 1597–1606 (2016).
14) Luo L., Patel A., Sinko B., Bell M., Wibawa J., Hadgraft J., Lane M. E., *Int. J. Pharm.*, **505**, 14–19 (2016).
15) Miki R., Ichitsuka Y., Yamada T., Kimura S., Egawa Y., Seki T., Juni K., Ueda H., Morimoto Y., *Eur. J. Pharm. Sci.*, **66**, 41–49 (2015).
16) Pérez-Madrigal M. M., Armelin E., Puiggalí J., Alemán C., *J. Mater. Chem. B.*, **3**, 5904–5932 (2015).
17) Fujie T., *Polym. J.*, **48**, 773–780 (2016).
18) Moreira J., Vale A. C., Alves N. M., *J. Mater. Chem. B.*, **9**, 3778–3799 (2021).
19) Flynn G. L., Yalkowsky S. H., Roseman T. J., *J. Pharm. Sci.*, **63**, 479–510 (1974).
20) Morimoto Y., Hatanaka T., Sugibayashi K., Omiya H., *J. Pharm. Pharmacol.*, **44**, 634–639 (1992).
21) Okamura Y., Kabata K., Kinoshita M., Saitoh D., Takeoka S., *Adv. Mater.*, **21**, 4388–4392 (2009).
22) Hatanaka T., Saito T., Fukushima T., Todo H., Sugibayashi K., Umehara S., Takeuchi T., Okamura Y., *Int. J. Pharm.*, **565**, 41–49 (2019).
23) Baxamusa S. H., Stadermann M., Aracne-Ruddle C., Nelson A. J., Chea M., Li S., Youngblood K., Suratwala T. I., *Langmuir*, **30**, 5126–5132 (2014).
24) Hatanaka T., Inuma M., Sugibayashi K., Morimoto Y., *Chem. Pharm. Bull.*, **38**, 3452–3459 (1990).
25) Zhang G., Zhang J., Zhou X., Shen D., *J. Appl. Polym. Sci.*, **88**, 973–979 (2003).
26) George S. C., Thomas S., *Prog. Polym. Sci.*, **26**, 985–1017 (2001).
27) Fujimori J., Yoshihashi Y., Yonemochi E., Terada K., *J. Control. Release*, **102**, 49–57 (2005).
28) Inoue Y., Atsumi Y., Kawamura A., Miyata T., *J. Membr. Sci.*, **588**, 117213 (2019).
29) Seki T., Harada S., Hosoya O., Morimoto K., Juni K., *Biol. Pharm. Bull.*, **31**, 163–166 (2008).
30) Hosoya O., Chono S., Saso Y., Juni K., Morimoto K., Seki T., *J. Pharm. Pharmacol.*, **56**, 1501–1507 (2010).
31) Seki T., Kiuchi T., Seto H., Kimura S., Egawa Y., Ueda H., Morimoto Y., *Biol. Pharm. Bull.*, **33**, 1915–1918 (2010).
32) Aguilella V., Kontturi K., Murtomäki L., Ramirez P., *J. Control. Release*, **32**, 249–257 (1994).
33) Cevc G., Vierl U., *J. Control. Release*, **141**, 277–299 (2010).
34) Kasting G. B., Miller M. A., LaCount T. D., Jaworska J., *J. Pharm. Sci.*, **108**, 337–349 (2019).
35) Riva E. R., Desii A., Sartini S., La Motta C., Mazzolai B., Mattoli V., *Langmuir*, **29**, 13190–13197 (2013).